Front. Optoelectron. 2016, 9(2): 194–205
DOI 10.1007/s12200-016-0623-2

REVIEW ARTICLE

Manipulating optical vortices using integrated photonics

Ning ZHANG[1], Kenan CICEK[1], Jiangbo ZHU[1], Shimao LI[2], Huanlu LI[3], Marc SOREL[3], Xinlun CAI (✉)[2], Siyuan YU (✉)[1,2]

1 Photonics Group, University of Bristol, Bristol BS8 1UB, UK
2 State Key Laboratory of Optoelectronic Materials and Technologies, Sun Yat-sen University, Guangzhou 510275, China
3 School of Engineering, University of Glasgow, Glasgow G12 8QQ, UK

Abstract Optical vortices (OVs) refer to a class of cylindrical optical modes with azimuthally varying phase terms arising either from polarization rotation or from the angular projection of the wave vector that at the quantum level corresponds to photon spin or orbital angular momenta. OVs have attracted the attention of researchers in many areas of optics and photonics, as their potential applications range from optical communications, optical manipulation, imaging, sensing, to quantum information. In recent years, integrated photonics has becomes an effective method of manipulating OVs. In this paper, the theoretical framework and experimental progress of integrated photonics for the manipulation of OVs were reviewed.

Keywords optical vortex, orbital angular momentum, angular grating, micro-ring resonator

1 Introduction

Optical vortices are a class of optical modes that have rotating polarization or phase variations, or both, around a central axis. Due to the rotating polarization or phase, the optical field in optical vortices (OVs) has at least one singularity, often at the center of rotation where the field cannot be defined, hence will be zero. OVs are one example of the so-called 'structured light' in which the spatial variation of field parameters including polarization, phase and wave vector results in fine structures in the distribution of field intensity. Due to the rotation in polarization and/or phase, photons in OVs carry spin and/or orbital angular momenta (SAM and OAM) [1–3].

The propagation of OVs, while obeying the general formulism of the Maxwell's equations, demonstrates interesting behaviors due to the spatially varying field distributions. The cylindrical symmetry often associated with OVs means that they are often best described using the cylindrical solutions of wave equation, i.e., the Bessel and Hankel mode sets. A linearly polarized set of such modes, the Lagurre-Gaussian (LG) modes, are well known to researchers [3]. The orthogonality between these modes, also often known as OAM beams (as being linearly polarized the photons only carry OAM due to their spiral phase fronts) have recently seen a high degree of interest in communications [4,5] because they potentially provide multiple independent communications channels in the same spatial channel using so-called OAM multiplexing. Very high amounts of data (up to 435 bit/s/Hz) have been successfully carried on one optical carried wave which is multiplexed into 52 numbers of such beams in a coaxial space channel [6].

In free space, the general laws of diffraction that links the near- and far-field distributions still apply, but the propagation can be dramatically different from that of the optical modes defined in a Cartesian coordinate. Interesting examples including the sharp focusing of a radially polarized vortex by a high numerical aperture (NA) lens that can produce a strongly axially (or longitudinally) polarized spot with a size smaller then allowed by the Abbe limit [7]. Such properties have been explored for ultra-high resolution imaging. The diffraction of the vortex beams can be higher than Gaussian beams and concerns have been raised of the consequences to some applications, in particular communications, as a more diffractive beam would require larger receiving apertures to effectively collect the energy [8]. The singularity on the axis of the beam is also not conducive to communications, as any receiver located on the axis would receive little energy.

In cylindrical waveguide or optical fibers, the problem of diffraction is overcome and here the prospects of long distance propagation with low energy loss are realistic. Recently optical fibers that support multiple optical vortex

Received February 6, 2016; accepted February 22, 2016

E-mail: caixlun5@mail.sysu.edu.cn, s.yu@bristol.ac.uk

modes have been reported [9,10]. The loss levels of some OAM fibers are comparable to widely used single mode fibers.

The fact that OVs carry angular momenta gives rise to interesting phenomena as they interact with matter. Beams carrying OAM have been shown to cause rotational movements of macroscopic particles including spin and orbital movements, and as such have been known as 'optical spanners' [11]. At microscopic levels, the interactions of photonic SAM with nanophotonic structures and with electronic states are hotly researched areas. Recently such interaction has been explored for quantum information storage [12], where high dimensional photonic superposition OAM states has been successfully stored and retrieved. There is also preliminary experiments involving the OVs in relativistic nonlinear processes [13].

Much of the generation, detection and manipulation of OVs has been implemented using bulk optical components, for example, by passing free space light beams through optical elements such as spiral phase plates (SPPs) [14,15], spatial light modulators (SLMs) [16], inhomogeneous birefringent elements [17], sub-wavelength gratings [18], nano-antennas [19], etc, which are either rigid (only one OAM state is generated, without switching or modulation capability) or very expensive. Electro-optically driven dynamic manipulation of OVs by means of SLM is a slow process. These components are cumbersome to use and with no clear route to scaling. They are also fragile and susceptible to disturbances, therefore lacking robustness, in particular as OV optics are highly sensitive to misalignment of the optical axis.

Compact, robust and efficient planar waveguide-based photonic integration technology has unique advantages in precision, reliability, miniaturization, and scalability compared to bulk optics. They can form photonic integrated circuits (PICs) that support the exploitation of OVs in various applications in ways that are not possible by means of bulk optics. A useful example is the transmitter and receiver devices in optical communications systems using OV mode multiplexing. While successful transmission experiments have been carried out using bulk optics, PICs will almost certainly be necessary for practical applications in real systems.

In this paper, the principles and recent progress of such integrated approaches to OV mode manipulation were presented and reviewed.

2 Integrated photonics for optical vortex generation and manipulation

2.1 OV modes

The cylindrical symmetry of OVs and the associated integrated photonic structures makes the theoretical treatment in polar or cylindrical coordinates a natural approach. This is defined so that the (ρ,φ) coordinates form the plane of a planar waveguide, and z is the central axis of the OV modes, as illustrated in Fig. 1.

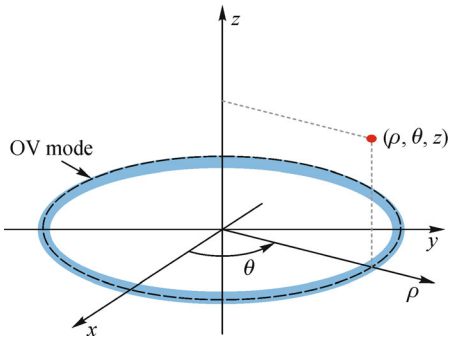

Fig. 1 Considered cylindrical coordinates

The z components of the electrical and magnetic fields satisfy the wave equation in cylindrical coordinates [20]:

$$\left(\frac{\partial^2}{\partial\rho^2}+\frac{1}{\rho}\frac{\partial}{\partial\rho}+\frac{1}{\rho^2}\frac{\partial^2}{\partial\theta^2}+\frac{\partial^2}{\partial z^2}+k_0^2n^2\right)\begin{matrix}H_z(\rho,\varphi,z)\\E_z(\rho,\varphi,z)\end{matrix}=0, \tag{1}$$

where n is the refractive index of the planar waveguide layer. The z components of the field have the following general form [21]:

$$\begin{matrix}H_z(\rho,\varphi,z)\\E_z(\rho,\varphi,z)\end{matrix}=R(\rho)\Psi(\varphi)Z(z). \tag{2}$$

For photonic integrated devices, the axial dependencies the planar waveguide mode distribution in the vertical direction:

$$\left(\frac{\partial^2}{\partial z^2}+k_0^2n^2\right)Z(z)=\beta^2, \tag{3}$$

where β is the axial wave vector. The azimuthal dependence takes the form of

$$\Psi(\varphi)=\exp(-\mathrm{j}l\varphi) \tag{4}$$

with the angular wave number, i.e., the topological charge $l = 2\pi nR/\lambda$, where R is the effective radius of the planar OV mode, and λ the wavelength. Due to the periodic boundary condition in the azimuthal direction $\Psi(\varphi)-\Psi(\varphi+2\pi)=l\times 2\pi$, l is limited to be an integer and is associated with the photonic OAM quantum number. The radial dependence has a Bessel/Hankel function form:

$$R(\rho)=a\mathscr{H}_l^{(1)}(\beta\rho)+b\mathscr{H}_l^{(2)}(\beta\rho), \tag{5}$$

where a and b are coefficients that can be determined by applying continuity condition at the interfaces.

Once the z-components of the field are established, the other in-plane field components can be obtained by well-known relations in order to give the full vector mode.

One particular example of the cylindrical vector modes confined in the planar waveguide is the whispering gallery mode (WGM) found propagating along the circumference of circular structures such as micro-discs and micro-rings. For WGMs, the azimuthal term in Eq. (4) indicates the azimuthal mode order with l being the number of wavelengths around the circle. It is also worth noted that WGMs have rotating polarization forced by the circular boundary condition.

The central problem with the manipulation of the OVs using integrated photonics is how energy couples between the confined optical modes in the planar waveguide and the free space OVs. This relies on photonic structures that embedded with cylindrically symmetric perturbations.

2.2 Cylindrical symmetric perturbations

The most well-known technique that can achieve in-plane guided mode to out-of-plane mode coupling is to introduce second-order Bragg grating along the propagation direction of the guided mode. To manipulate OVs, the Bragg grating needs to have the same cylindrical symmetry. Since the in-plane OV modes can propagate along the radial direction (inward/outward) or azimuthal direction (clockwise (CW)/counter clockwise (CCW)), the second order Bragg grating can be introduced to integrated photonic structures through refractive index modulation in the radial direction (i.e., in concentric circular patterns) or in the azimuthal direction (i.e., periodic structure on a circular waveguide to form angular gratings).

Concentric circular gratings have been used in some surface emitting lasers to achieve higher efficiency and larger lasing-area [22–25]. The first example of using circular gratings in OV manipulation is an integrated circuit fabricated on silicon [26]. In this circuit, a group of configured waveguides converges radially toward the center, where the second-order circular gratings couple the light out of the plane into the vertical direction (or vice versa for receiving). The relative phase between the converging waveguides determines the topological charge of the emitted beam and can be adjusted by on-chip phase shifters that operate on the thermos-optic effect of silicon. This integrated circuit can support the emission and reception of OVs with multiple topological charges through implementing an on-chip planar optical Fourier transform circuit to convert between spatial phase domain and real spatial domain.

In such radial excitation schemes, to achieve high-quality OV beams with pure topological charge relies on the accurate phase control between the excitation waveguides. To achieve high topological charge (l) values, a large number ($2l$) of excitation waveguides are needed.

As the radially propagating in-plane mode has a Bessel function distribution along the radial direction, the optimised second-order circular gratings in general should satisfy a distribution conformal to the phase alternation of the Bessel/Hankel functions along the radial direction, in particular for smaller devices [27,28]. Only at the large radius limit the circular gratings can be equidistance or periodic.

Angular gratings can provide good azimuthal phase accuracy when coupling the in-plane modes into vertical emitting modes. Prior to manipulating OVs, angular gratings were used in cylindrically symmetric integrated photonic structures, including micro disc and ring lasers, to achieve single-mode lasing [29–31]. Recently, angular gratings were introduced to silicon ring resonator to generate OVs carry photonic OAM [32]. In this scheme, since the planar waveguide is curved as a ring, the wavefront of the radiated beams is transformed into a helix, i.e., the phase front of OV beams. The planar ring resonator support azimuthally traveling WGMs and the second order angular gratings patterned on the inner sidewall of the ring resonator scatter the confined planar modes to the out-of-plane OV beams. The topological charge of the emitted OV beam, hence the quantum number of the photonics OAM it carries, is determined by the topological charge of the WGM and the number of the grating periods. As the periodic boundary condition along azimuthal direction automatically set the topological charge of the in-plane WGM mode to be an integer, high OAM purity can be obtained.

2.3 Theoretical analyzing methods

Different methods have been used to analyze photonic structures embedded with circular or angular gratings, including coupled-mode theory (CMT) [33–35] and finite-differential time-domain (FDTD) numeric method [36]. The FDTD method is a straightforward tool but the physical interaction of modes in the perturbed photonic structures can be hard to discern from the simulation result. A dipole model [37] that uses dipole oscillators to represent the light scattered from grating elements has been used to provide a good prediction of the emitted beam, however it is incapable of describing the physical interaction inside the structure as few structural parameter can be included in the calculation process.

In the initial research [32], CMT was used to derive the phase matching condition in the azimuthal direction. Recently, CMT has been extended to provide anew theoretical method for analyzing the interaction between OV and cylindrical structures [38]. In this method, the conventional coupled mode equations describing the 1D gratings (such as those in distributed feedback (DFB) lasers) [39–42]are redeveloped under the cylindrical coordinates to analyze the interactions between cylindrical modesinduced by circular and angular gratings.

Take the analyses of the mode coupling process in the ring resonator with angular gratings on its sidewall as an example. Fist the refractive index distribution within the perturbed region (Δn) is expressed using spatial Fourier

expansion:

$$\Delta n = \sum_{\substack{f=-\infty \\ f\neq 0}}^{+\infty} \frac{n_1^2 - n_2^2}{\pi f R} \sin(\pi f r) \exp\left(\mathrm{j}\frac{2\pi f R}{\Lambda}\varphi\right), \quad (6)$$

where n_1 and n_2 are the two different refractive indices within the perturbation region, f the Fourier expansion coefficient, r the grating duty ratio, R the mean radius of the resonator, and Λ the period of the gratings. Then the azimuthal propagating mode is expanded in partial waves since the interaction between the mode and the angular gratings decomposes the azimuthal dependence of the mode. The topological charge of each partial wave is expressed as

$$l_m = l + \frac{2\pi R}{\Lambda} m, \quad (7)$$

where m is the order of the partial wave. For second order gratings, the grating period is set to the optical wavelength of the guided mode in the waveguide, hence $m = -2$ enables the condition of

$$l_{-2} = l - \frac{4\pi R}{\Lambda} = -l. \quad (8)$$

Under this condition, partial waves with the order of $-2 < m < 0$, i.e., $m = -1$, radiate power away from the perturbed structure, while the orders of $m < -2$ and $m > 0$ are decaying within the planar region, and $m = 0$ and $m = -2$ remain as the coherent guided waves propagating in CW and CCW directions, respectively. In this way, the mode coupling analyses in this angular-grating-perturbed structure is transformed into the analyses about the coupling process between different partial waves. Meanwhile, the calculation of the out-of-plane OV mode equals to the calculation of the radiated partial wave ($m = -1$).

Generally, the coupling process between different partial waves can be summarized as: the two in-plane CW and CCW propagating waves are the main sources that excite the other partial waves, which will in turn couple energy back to the source waves. The coupled equations developed to describe this process are as follows:

$$\frac{\partial A(\varphi)}{\partial \varphi} + A(\varphi)(-\mathrm{j}\delta - \mathrm{j}\xi_1 - \alpha) = \mathrm{j}(\kappa_{-2} + \xi_2)B(\varphi), \quad (9)$$

$$-\frac{\partial B(\varphi)}{\partial \varphi} + B(\varphi)(-\mathrm{j}\delta - \mathrm{j}\xi_3 - \alpha) = \mathrm{j}(\kappa_2 + \xi_4)A(\varphi). \quad (10)$$

In the equations above, $A(\varphi)$ and $B(\varphi)$ are slowly-varying complex functions representing the azimuthal variations of the waves traveling CW and CCW, respectively, δ is the deviation of the topological charge of the planar OV mode, α is the gain/loss experienced by the waves, $\kappa_{2/-2}$ is the back-scattering coefficients, and factors ξ_1 to ξ_4 are the Streifer terms [41,42]. ξ_1 represents the coupling from all the partial waves excited by the CW propagating wave back to itself, and ξ_3 represents the coupling from all the partial waves excited by the CCW propagating wave back to itself; ξ_2 represents the coupling from the partial waves excited by the CW propagating wave to the CCW propagating wave, and ξ_4 represents the coupling from the partial waves excited by the CCW wave to the CW wave. With appropriate boundary conditions applied at $\varphi = 0$ and $\varphi = 2\pi$, $A(\varphi)$ and $B(\varphi)$ can thus be solved, leading to the calculation of each partial wave. Since the values of the Streifer terms are determined by the Fourier expansion of the perturbed refractive index as shown in Eq. (6) which is highly structure dependent, the effects of the structural parameters on the coupling process and emitted partial wave can also be analyzed.

This theoretical analysis is also applicable to circular gratings. The main difference is about the spatial decomposition of the perturbed refractive index distribution. As explained above, the radial dependence of the OV mode has a Bessel/Hankel function form, hence the Bessel-Fourier series should be used to decompose the circular gratings. Correspondingly, since in structures with circular gratings the planar OV mode travels along the radial direction, the interaction between the mode and the circular perturbations decomposes the radial dependence of the mode rather than the azimuthal dependence. The inward and outward traveling waves are the main sources that excite other partial waves and under the same analyzing process for the angular-grating-perturbed structure, similar coupled equations can be obtained for the radial variations of the inward and outward traveling waves. Large radius approximation [43] can be used to solve the coupled equations and partial waves analytically.

The potential of this CMT based method to analyze and optimise integrated OV manipulation devices embedded with cylindrically symmetric perturbations has been successfully proved through device optimisation, as described below.

2.4 Typical OVs manipulation devices

2.4.1 Compact OV beam emitter/receiver

The micro-ring resonator based OV beam emitter [32] is shown in Fig. 2(a).

This device is fabricated on a silicon-on-insulator (SOI) substrate. The second-order angular grating, patterned on the inner sidewall of the ring resonator, couple the energy from the planar WGMs to the vertically radiating OV beam, with the topological charge of the radiated OV beam satisfying:

$$l_{\mathrm{rad}} = \mathrm{sign}(l)(l - q), \quad (11)$$

where sign(l) = + or − represents the CW or CCW WGM

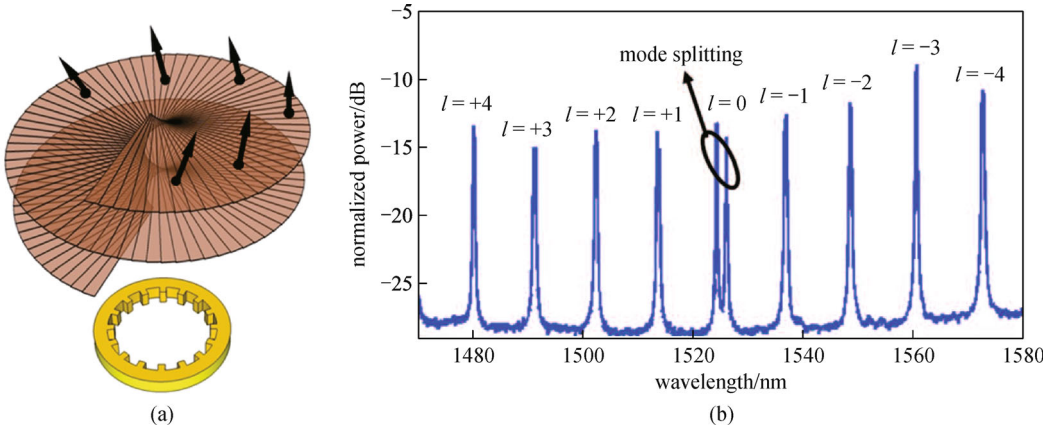

Fig. 2 Integrated OV beam emitter [32]. (a) Structure of the OV emitter with input bus waveguide not shown for simplicity; (b) radiation spectrum of the OV emitter

mode, and q the number of grating periods. This relationship has been derived in the supplementary material of Ref. [32] and analytical proven using CMT in the theoretical method [38] explained above. The intrinsic periodic boundary condition along the azimuthal direction in the ring resonator clearly defines the topological charge of the emitted OV beam, resulting in a good OV mode purity. The emission characteristics of this device (R = 7.5 μm, q = 72) with scanning input wavelength is shown in Fig. 2(b), where each resonance corresponds to a distinctive l_{rad}. The mode splitting in the spectrum results from the back-scattering between the CW and CCW propagating waves, as introduced in Eqs. (9) and (10) above.

Variable l_{rad} is either achievable by tuning the injected laser wavelength to excite various l, or, as in a reconfigurable device [44], by electrically driven thermo-optical effect to switching between different l_{rad} when the optical wavelength is fixed.

The emitted OV beam is a cylindrical OV beam as its state of polarization (SOP) maintains the cylindrical symmetry of both the angular gratings and the rotating SOP of the in-plane WGMs. Generally speaking, the SOP of the radiated OV beam is a combination of radial and azimuthal polarizations but for the l_{rad} = 0 mode where mode splitting is obvious, one of the split peak exhibits pure radial polarization and the other with pure azimuthal polarization [45]. On the other hand, the OV beam can be described as the superposition of two orthogonal scalar vortices [46]: one is right-hand circularly polarized (RHCP) with topological charge of l_{rad} + 1, while the other is left-hand circularly polarized (LHCP) with topological charge of $l_{\mathrm{rad}}-1$. This fact is critical to detecting the OAM order carried by the emitted OV beam and also in determining the OAM order carried by an input OV beam when the same device is used as a receiver.

By the principle of reciprocity, when the device is used as an OV beam receiver, the second-order angular gratings serve a similar but reversed role as in the emitting process, i.e., to couple the energy of an incoming vertical propagating OV beam to the in-plane propagating WGMs. The layout of the receiving process is shown in Fig. 3(a).

When the device is illuminated with an incident OV beam, part of it is diffracted by the angular gratings and become confined inside the resonator as a WGM. The selection rule in receiving is

$$\pm(l-q) = l_{\mathrm{OAM}} - l_{\mathrm{SAM}}, \tag{12}$$

where l_{OAM} is the quantum number of the photonic OAM carried by the incident OV beam and l_{SAM} is the polarization direction which equals to + 1 for RHCP beam and − 1 for LHCP beam. The sign before $(l-q)$ results from the fact that both CW and CCW traveling planar OV mode can be excited by the same incident OV beam. The excited CW traveling mode $[+(l-q)]$ is collected at the CW port and the excited CCW traveling mode $[-(l-q)]$ is collected at the CCW port, respectively. According to this selection rule, when an LHCP (l_{SAM} = − 1) OV beam carrying OAM l_{OAM} = − 4 incidents on this ring resonator, CW propagating planar OV mode with topological charge $l = -4-(-1)+q$ can be excited inside the waveguide and collected at the CW port, while CCW propagating planar OV mode with topological charge $l = -[-4-(-1)]+q$ can be excited inside the waveguide and collected at the CCW port. The experimental result of the receiving function of this device is shown in Fig. 3(b), where an LHCP OV beam incidents the receiver and the received energy is collected at the CW port. Though high side mode suppression ratio (SMSR) has not been achieved yet, the receiving function and mechanism explained in Eq. (12) has been successfully proved.

Though the resonant cavity of this compact OV beam emitter/receiver enables advantage in achieving well-defined and easily tuned topological charge, it also brings a disadvantage which is the one-to-one correspondence between the topological charge and the optical wavelength

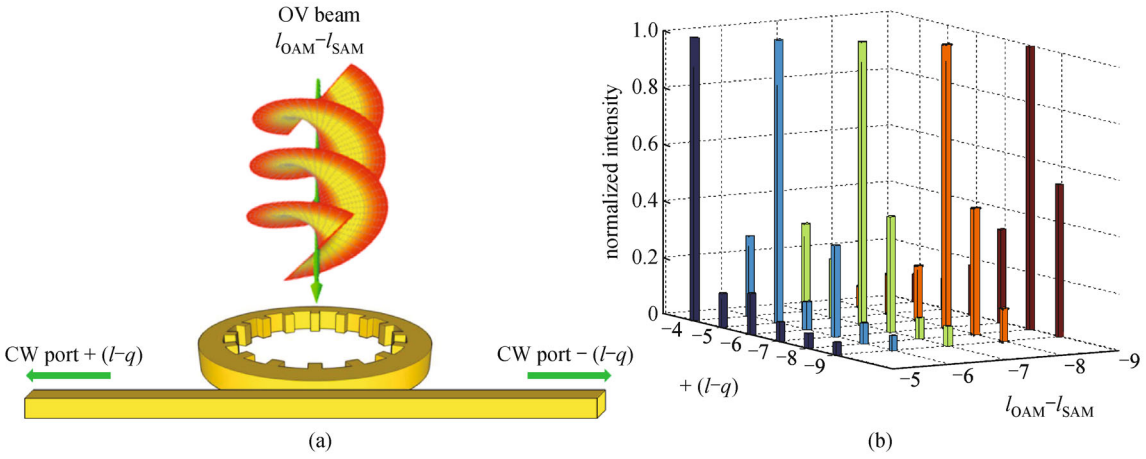

Fig. 3 Integrated OV beam receiver. (a) Layout of the receiving process; (b) experimental result of the OV beam receiver. An LHCP OV beam incidents the receiver and the received energy is collected at the CW port

(or frequency), which makes the multiplexing and super position of photonic OAM states difficult. Meanwhile, optimisations for this corrugated ring resonator are needed. For example, the radiation efficiency – energy of the radiated OV beam over that of the input laser – needs to be increased, and higher mode purity is also preferable.

2.4.2 Efficiency-optimized OV beam emitter

To increase the efficiency of the OV beam emitter introduced above, one can reuse the energy emitted to other directions rather than the preferred output direction, or increase the in-plane to out-of-plane coupling efficiency.

As the second order grating has no preference over up- or down-ward emission, approximately equal amount of energy is coupled into each direction. To achieve higher upward emission efficiency, reusing the down-ward energy is an effective approach. In the device shown in Fig. 4(a), a metal layer with high reflectivity is introduced under the silicon ring resonator, fabricated using a wafer bonding technique. The thickness of the buffer layer between the silicon resonator and the metal layer is set as a multiple of half the optical wavelength. According to the calibrated radiation spectrum (Fig. 4(b)) measured from both the original and the new device, the radiation efficiency has been significantly increased for as much as 7 dB. As the old device has an emission efficiency of about 10%, the new device has an emission efficiency of $>50\%$.

To increase the in-plane to out-of-plane coupling efficiency of the grating, the impact of grating structural parameter on the coupling efficiency needs to be studied. Using the CMT-based method of Section 2.3 to simulate the device, a relationship between grating duty ratio (the ratio of the grating tooth width over its period) and the rectangular grating's coupling coefficienties found to achieve maximum near 50% duty ratio, as shown in Fig. 5(a).

In the original device [32], the distribution of grating

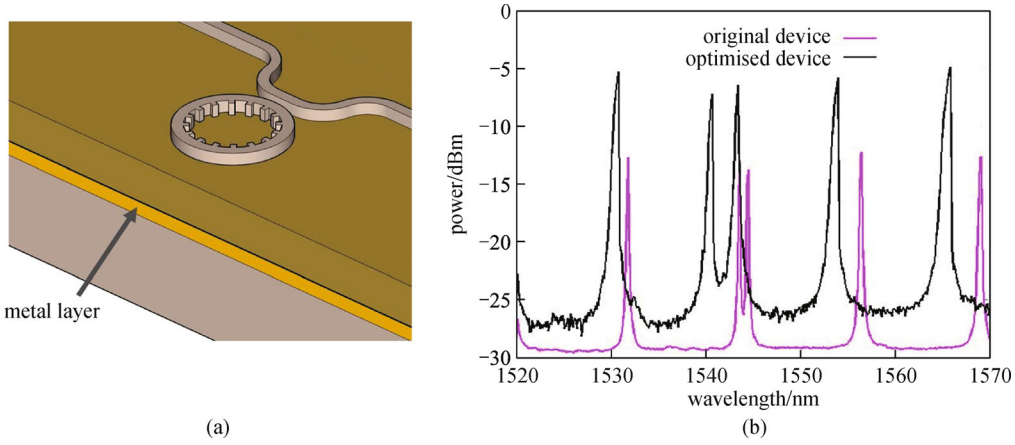

Fig. 4 Efficiency-optimised OV beam emitter. (a) Structure of the optimised device; (b) radiation spectrum comparison

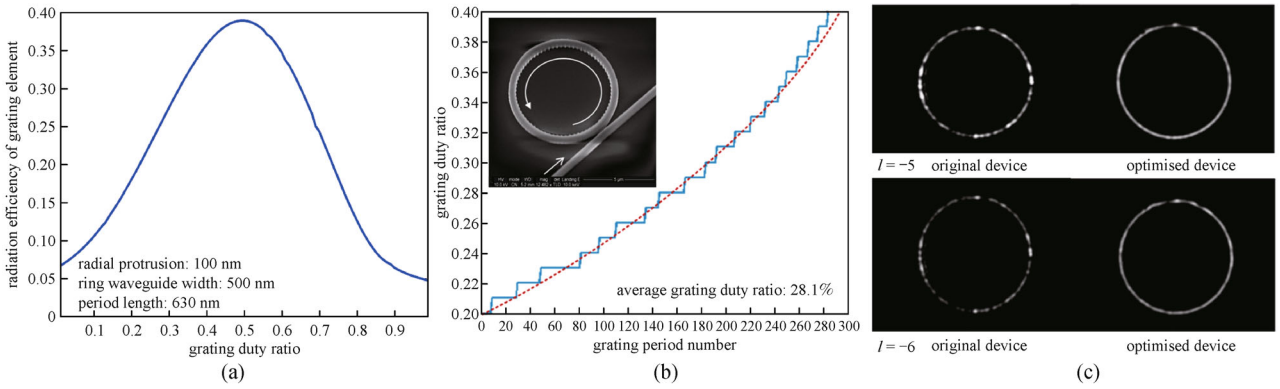

Fig. 5 Efficiency- and near-field-optimised OV beam emitter. (a) Relationship between grating duty ratio and its radiation efficiency; (b) grating duty ratio in the optimised device; (c) near-field intensity distribution comparison

duty ratio is uniform (~10%). As energy is gradually extracted from the ring waveguide, a non-uniform near-field intensity distribution results from the decaying energy in the waveguide. This phenomenon will be further deteriorated if the grating's coupling coefficient is increased. A non-uniform near-field will deteriorate the mode purity as the azimuthal amplitude variation creates side modes.

To optimise the device for both increased emission and more uniform near-field, the grating duty ratio (hence the coupling coefficient)at each period is varied according to

$$r_1 = \frac{r_{i+1}}{1 + r_{i+1}}, i = 1,2,...,q-1, \qquad (13)$$

where r_i is the grating duty ratio in the ith period. According to this design principle, the distribution of grating duty ratio in the optimized device gradually increases exponentially from ~20% to ~40% following Eq. (13), as shown in Fig. 5(b) (the red curve). In practice, the grating is divided into small sections within each the value of r_i is constant with the same duty ratio (the blue curve). Fabricated device not only demonstrate increased total emission efficiency(from ~10% to ~35%) as expected, the near-field intensity distribution (Fig. 5(c)) is also significantly more uniform, which may result in a better OV mode purity [47].

2.4.3 OV beam emitter generating photonic OAM superposition states

High dimensional superposition OAM states could be very useful for quantum information systems. Based on the above device principle, by superimposing angular gratings with different periods, the device should emit OV beams carrying photonic OAM superposition states.

The concept is illustrated in Fig. 6(a), where R is the mean radius of the resonator and a is the amplitude of the sinusoidal gratings. The profiles of two sets of angular gratings with period Λ_1 and Λ_2 are added, generating a beat pattern that modulates the original gratings periodically. The number of the period in the beat pattern is determined by the difference in the number of elements in the two sets of gratings, which is also the topological charge difference of the superposition OAM states carried by the emitted OV beam, as the relationship between the topological charge of the in-plane OV mode and that of the out-of-plane OV mode in Eq. (11) is maintained. The measured topological charge spectra emitted from the 'two-beat' and 'three-beat' grating devices are shown in Fig. 6(b). The weights of the two composition OAM states are nearly equal, as the sinusoidal gratings have the same amplitude. Similar to that in the single OV device, through tuning the wavelength, the topological charges of the super-positional OAM states can change synchronously, but maintains the difference of 2 or 3. This novel device is a promising source for quantum information and optical manipulation, where super-positional OAM states would be needed.

2.4.4 Broadband OV beam emitter and OAM multiplexer

The one-to-one correspondence between the topological charge of the emitted OV beam and the optical wavelength in the resonant cavity-based OV beam emitter can be broken when the ring resonator is not enclosed, which is achievable through using an arc waveguide. This results in a Ω-shaped OV beam emitter as shown in Fig. 7(a). The input waveguide connects to an arc waveguide with second-order angular gratings. This arc waveguide has arc radius R and arc angle $2\pi - \alpha$, with an open notch angle of α.

The relationship between the topological charge of the out-of-plane and in-plane OV modes in this Ω-shaped emitter is the same as that in the resonant cavity-based emitter. The difference is that in the Ω-shaped emitter there is no resonance. In this way, this Ω-shaped emitter is a broadband OV beam emitter as the emission efficiency

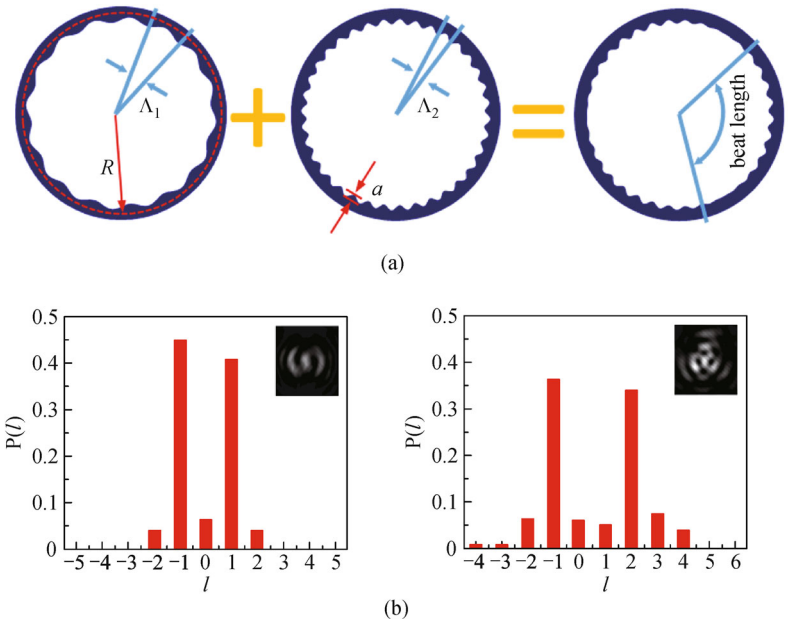

Fig. 6 OV beam emitter that can generate superposition OAM states [48]. (a) Concept of superimposed gratings; (b) radiation spectra of OV beams emitted from two- and three-beat gratings emitters

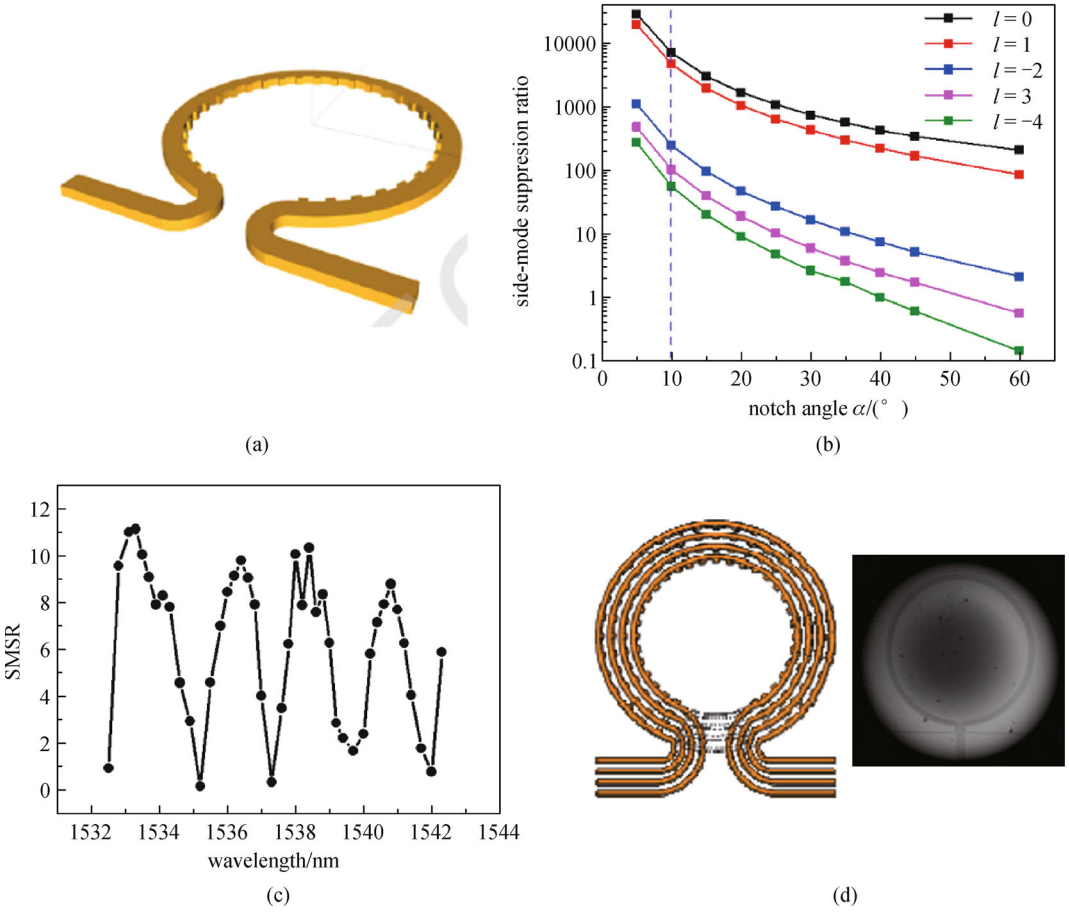

Fig. 7 Ω-shaped OV beam emitter. (a) Schematic figure of the Ω-shaped emitter; (b) relationship between SMSR and notch angle; (c) measured SMSR from a fabricated device; (d) schematic figure and micrograph of the Ω-shaped OAM multiplexer

hardly changes with wavelength. The lack of resonance, however, also removes the round-trip phase constraint, thus the topological charge of the OV mode could be non-integer, giving rise to fractional photonic OAM. This is shown in the OAM SMSR (power of the dominant OV mode over the second highest mode) measured from a fabricated device in Fig. 7(c). At wavelengths corresponding to the would-be resonant modes if the ring were enclosed, one dominant mode is emitted with good SMSR, while between these wavelengths two equal modes would be emitted when SMSR drops to 0 dB. A wavelength range of >1 nm within which SMSR maintains a reasonable value (1 – 2 dB down from maximum) can be achieved.

The notch angle of the arc waveguide (where emission is missing hence imparts an amplitude modulation on the near-field) could also deteriorate mode purity. Figure 7(b) shows the SMSR as a function of the notch angle α at wavelengths corresponding to different dominant topological charge, which is calculated using the dipole model. It can be seen that the SMSR deteriorates as the notch angle increases. For the same notch angle, higher order OAM suffers from lower SMSR. If the purity criteria of the photonic OAM carried by the OV beam is set as SMSR >20 dB for l_{rad} up to 4, the notch angle in the Ω-shaped OV emitter should be limited to within 10°.

The opening notch in the waveguide allows Ω-shaped emitters with different arc radii to be nested coaxially as in Fig. 7(d), enabling an OAM multiplexer. By integrating four Ω-shaped OV beam emitters coaxially, 8-channel OAM multiplexing can be achieved as each device can be excited in the CW or CCW direction.

2.4.5 Resonant OAM multiplexer

Exploiting the existence of higher transverse order WGMs, an OAM multiplexer based on micro-ring resonator is proposed. As shown in Fig. 8(a), this micro-ring cavity has a multimode waveguide that support TE0 and TE1 modes. Each will form a set of resonances due to their different propagation constants, with different free spectral range (FSR). By way of Vernier effect, they will coincide at one particular wavelength. The coupling from the WGM mode to the vertical emitting OV mode happens by the same selection rule explained in Eq. (11), therefore at that wavelength, two OV modes with different topological charges can be emitted.

To address these modes, two bus waveguides (I and II) with different width are designed to selectively excite the TE0 and TE1 mode, respectively. As each bus waveguide has propagation constant synchronised with one of the ring waveguide modes, it will only excite one OV mode with one topological charge. As each bus waveguide has two input ports and both CW and CCW traveling modes can be excited inside the microring, this scheme can allow multiplexing of up to four different OAM states.

The radiation spectra for the TE0 mode excited by bus waveguide I and the TE1 mode excited by bus waveguide II are measured from a fabricated device as shown in Fig. 8(b). The wavelength where both modes are excited is where OAM multiplexing can be achieved. Based on this scheme, more OAM multiplexing channels are possible with a wider ring waveguide that support more transverse modes.

2.4.6 Active OAM beam emitter

A totally different approach is afforded by vertical cavity surface emitting lasers (VCSELs). VCSELs are highly power efficient and capable of emitting high-quality Gaussian-like beams with well-controlled linear polarization. Recently a novel approach to generate specific OAM carrying OV beams by integrating micro-sized SPPs in the aperture of commercially available VCSELs has been reported [49].

The structure of a VCSEL (8.5 μm diameter) integrated with SPP is illustrated in Fig. 9. Without the SPP, the

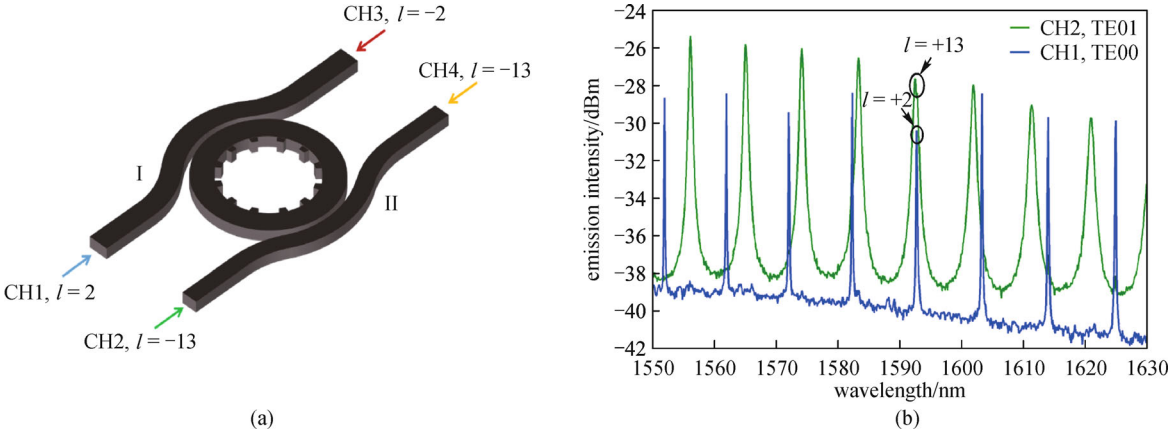

Fig. 8 OAM multiplexer. (a) Structure of the multiplexer; (b) radiation spectra of the fundamental and second-order modes from input port CH1 and CH2, respectively

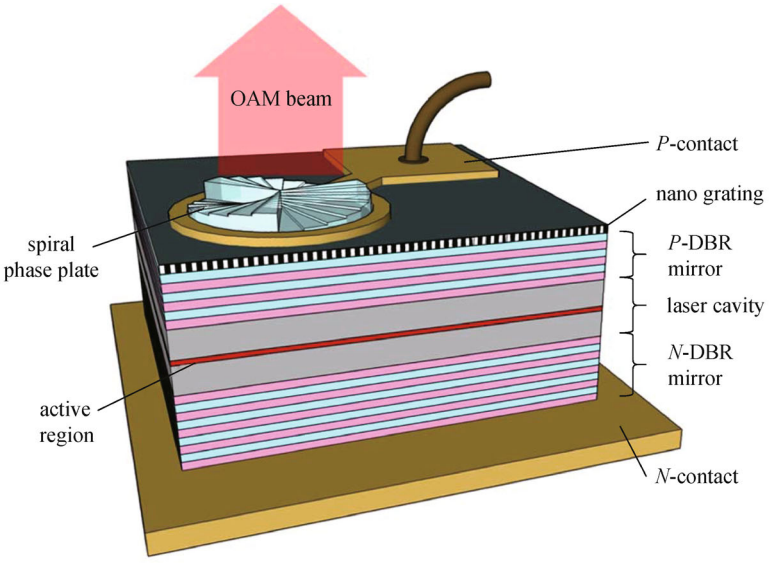

Fig. 9 Structure of a VCSEL OV emitter integrated with SPP [49]

VCSEL emits linearly polarized Gaussian beam at a wavelength of 860 nm. The SPP on the aperture imparts the helical phase term $\exp(jl\varphi)$, converting the Gaussian beam into an OV beam. This SPP is patterned in a deposited SiN_x layer using a focused ion beam (FIB) etching technique. Single as well as superposition OAM states have been experimentally achieved – the latter by fabricating multiple SPPs in the same device.

3 Conclusions

In recent years, methodologies and devices based on the concept of photonic integration has been developed that enable significant progress in innovative emitters and receivers of optical vortex beams, realizing functions ranging from high purity single mode emission and mode selective receiving, super positional mode emission, and multiplexing. Device performance has been significantly improved to achieve high emission efficiency and high mode purity.

The photonic integration based schemes offer several very important advantages that allow the engineering and dynamic control of the OV mode near- and far-field including amplitude, phase and state-of-polarization distributions, which is difficult to achieve by free space bulk optics. Such capabilities are potentially very useful in the research of singular optics and structure light. The photonic integrated devices are compact, precise, stable, robust, reliable, and easily reconfigurable by on-chip electrical control, and thus opens up opportunities in a range of important applications in optical communications, quantum technology, imaging and sensing, etc.

Acknowledgements The authors wish to acknowledge support by the National Basic Research Program of China (No. 2014CB340000), the National Natural Science Foundation of China-Key Research Project (Grant No. 61490715), and the EU Horizon2020 program under project ROAM.

References

1. Poynting J H. The wave motion of a revolving shaft, and a suggestion as to the angular momentum in a beam of circularly polarised light. Proceedings of the Royal Society of London, Series A, Containing Papers of a Mathematical and Physical Character, 1909, 82(557): 560–567
2. Beth R A. Mechanical detection and measurement of the angular momentum of light. Physical Review, 1936, 50(2): 115–125
3. Allen L, Beijersbergen M W, Spreeuw R J, Woerdman J P. Orbital angular momentum of light and the transformation of Laguerre-Gaussian laser modes. Physical Review A, 1992, 45(11): 8185–8189
4. Wang J, Yang J Y, Fazal I M, Ahmed N, Yan Y, Huang H, Ren Y, Yue Y, Dolinar S, Tur M, Willner A E. Terabit free-space data transmission employing orbital angular momentum multiplexing. Nature Photonics, 2012, 6(7): 488–496
5. Bozinovic N, Yue Y, Ren Y, Tur M, Kristensen P, Huang H, Willner A E, Ramachandran S. Terabit-scale orbital angular momentum mode division multiplexing in fibers. Science, 2013, 340(6140): 1545–1548
6. Wang J, Liu J, Lv X, Zhu L, Wang D, Li S, Wang A, Zhao Y, Long Y, Du J, Hu X, Zhou N, Chen S, Fang L, Zhang F. Ultra-high 435-bit/s/Hz spectral efficiency using N-dimentional multiplexing and modulation link with pol-muxed 52 orbital angular momentum (OAM) modes carrying Nyquist 32-QAM signals. In: Proceedings of European Conference on Optical Communication (ECOC), 2015
7. Shu J, Chen Z, Pu J, Zhu J, Liu D. Tight focusing of partially coherent and radiallly polarized vortex beams. Optics Communications, 2013, 295(10): 5–10

8. Edfors O, Johansson A J. Is orbital angular momentum (OAM) based radio communication an unexploited area? IEEE Transactions on Antennas & Propagation, 2012, 60(2): 1126–1131
9. Brunet C, Vaity P, Messaddeq Y, LaRochelle S, Rusch L A. Design, fabrication and validation of an OAM fiber supporting 36 states. Optics Express, 2014, 22(21): 26117–26127
10. Ung B, Vaity P, Wang L, Messaddeq Y, Rusch L A, LaRochelle S. Few-mode fiber with inverse-parabolic graded-index profile for transmission of OAM-carrying modes. Optics Express, 2014, 22 (15): 18044–18055
11. Padgett M J, Allen L. The angular momentum of light: optical spanners and the rotational frequency shift. Optical and Quantum Electronics, 1999, 31(1): 1–12
12. Ding D S, Zhang W, Zhou Z Y, Shi S, Xiang G Y, Wang X S, Jiang Y K, Shi B S, Guo G C. Quantum storage of orbital angular momentum entanglement in an atomic ensemble. Physical Review Letters, 2015, 114(5): 050502-1–050502-5
13. Han Y J, Liao G Q, Chen L M, Li Y T, Wang W M, Zhang J. High-order optical vortex harmonics generated by relativistic femtosecond laser pulse. Chinese Physics B, 2015, 24(6): 065202
14. Gibson G, Courtial J, Padgett M, Vasnetsov M, Pas'ko V, Barnett S, Franke-Arnold S. Free-space information transfer using light beams carrying orbital angular momentum. Optics Express, 2004, 12(22): 5448–5456
15. Heckenberg N R, McDuff R, Smith C P, White A G. Generation of optical phase singularities by computer-generated holograms. Optics Letters, 1992, 17(3): 221–223
16. Beijersbergen M W, Coerwinkel R P C, Kristensen M, Woerdman J P. Helical-wavefront laser beams produced with a spiral phaseplate. Optics Communications, 1994, 112(5-6): 321–327
17. Marrucci L, Manzo C, Paparo D. Optical spin-to-orbital angular momentum conversion in inhomogeneous anisotropic media. Physical Review Letters, 2006, 96(16): 163905-1–163905-4
18. Biener G, Niv A, Kleiner V, Hasman E. Formation of helical beams by use of Pancharatnam-Berry phase optical elements. Optics Letters, 2002, 27(21): 1875–1877
19. Yu N, Genevet P, Kats M A, Aieta F, Tetienne J P, Capasso F, Gaburro Z. Light propagation with phase discontinuities: generalized laws of reflection and refraction. Science, 2011, 334(6054): 333–337
20. Snyder A W, Love J D. Optical Waveguide Theory. Berlin: Springer, 1983, 12(3): 1–37
21. Wu C, Makino T, Glinski J, Maciejko R, Najafi S I. Self-consistent coupled-wave theory for circular gratings on planar dielectric waveguides. Journal of Lightwave Technology, 1991, 9(10): 1264–1277
22. Jordan R H, Hall D G, King O, Wicks G, Rishton S. Lasing behavior of circular grating surface-emitting semiconductor lasers. Journal of the Optical Society of America B, 1997, 14(2):449–453
23. Barlow G F, Shore A, Turnbull G A, Samuel I. Design and analysis of a low-threshold polymer circular-grating distributed-feedback laser. Journal of the Optical Society of America B, 2004, 21(12): 2142–2150
24. Scheuer J, Green W M, DeRose G A, Yariv A. Lasing from a circular Bragg nanocavity with an ultrasmall modal volume. Applied Physics Letters, 2005, 86(25): 251101-1–251101-3
25. Scheuer J, Green W M, Derose G A, Yariv A. InGaAsP annular Bragg lasers: theory, applications, and modal properties. IEEE Journal of Selected Topics in Quantum Electronics, 2005, 11(2): 476–484
26. Doerr C R, Buhl L L. Circular grating coupler for creating focused azimuthally and radially polarized beams. Optics Letters, 2011, 36 (7): 1209–1211
27. Scheuer J. Radial Bragg lasers: optimal design for minimal threshold levels and enhanced mode discrimination. Journal of the Optical Society of America B, 2007, 24(9): 2178–2184
28. Liang G, Liang H, Zhang Y, Li L, Davies A G, Linfield E, Yu S F, Liu H C, Wang Q J. Low divergence single-mode surface-emitting concentric-circular-grating terahertz quantum cascade lasers . Optics Express, 2013, 21(26): 31872–31882
29. Fujita M, Baba T. Microgear laser. Applied Physics Letters, 2002, 80(12): 2051–2053
30. Zhang Z, Dainese M, Wosinski L, Qiu M. Resonance-splitting and enhanced notch depth in SOI ring resonators with mutual mode coupling. Optics Express, 2008, 16(7): 4621–4630
31. Arbabi A, Goddard L L. Grating assisted mode coupling in microring resonators. In: Proceedings of IEEE Photonics Conference (IPC). 2013, 434–435
32. Cai X, Wang J, Strain M J, Johnson-Morris B, Zhu J, Sorel M, O'Brien J L, Thompson M G, Yu S. Integrated compact optical vortex beam emitters. Science, 2012, 338(6105): 363–366
33. Greene P L, Hall D G. Effects of radiation on circular-grating DFB lasers I. coupled-mode equations. IEEE Journal of Quantum Electronics, 2001, 37(3): 353–364
34. Huy K P, Morand A, Amans D, Benech P. Analytical study of the whispering-gallery mode in two-dimensional microgear cavity using coupled-mode theory. Journal of the Optical Society of America B, 2005, 22(8): 1793–1803
35. Sun X, Yariv A. Modal properties and modal control in vertically emitting annular Bragg lasers. Optics Express, 2007, 15(25): 17323–17333
36. Fujita M, Baba T. Proposal and finite-difference time-domain simulation of whispering gallery mode microgear cavity. IEEE Journal of Quantum Electronics, 2001, 37(10): 1253–1258
37. Zhu J, Cai X, Chen Y, Yu S. Theoretical model for angular grating-based integrated optical vortex beam emitters. Optics Letters, 2013, 38(8): 1343–1345
38. Yu S, Cai X, Zhang N. High index contrast integrated optics in the cylindrical coordinate. In: Proceeding of Society of Photo-Optical Instrumentation Engineers (SPIE) Conference Series, 2015
39. Streifer W, Scifres D R, Burnham R D. Analysis of grating-coupled radiation in GaAs:GaAlAs lasers and Waveguides-I. IEEE Journal of Quantum Electronics, 1976, 12(7): 422–428
40. Streifer W, Burnham R D, Scifres D R. Analysis of grating-coupled radiation in GaAs: GaAIAs lasers and waveguides II. blazing effects. IEEE Journal of Quantum Electronics, 1976, 12(8): 494–499
41. Streifer W, Scifres D R, Burnham R D. Coupled wave analysis of DFB and DBR lasers. IEEE Journal of Quantum Electronics, 1977, 13(4): 134–141
42. Hardy A, Welch D F, Streifer W. Analysis of second-order gratings. IEEE Journal of Quantum Electronics, 1989, 25(10): 2096–2105

43. Watson G N. A treatise on the theory of Bessel functions. Nature, 1945, (3955):190–191
44. Strain M J, Cai X, Wang J, Zhu J, Phillips D B, Chen L, Lopez-Garcia M, O'Brien J L, Thompson M G, Sorel M, Yu S. Fast electrical switching of orbital angular momentum modes using ultra-compact integrated vortex emitters. Nature Communications, 2014, 5: 4856
45. Liu J, Li S, Zhu L, Klitis C, Chen Y, Wang A, Li S, Long Y, Zheng S, Chen S, Sorel M. Demonstration of few mode fiber transmission link seeded by a silicon photonic integrated optical vortex emitter. In: Proceeding of European Conference on Optical Communication (ECOC), 2015
46. Moreno I, Davis J A, Ruiz I, Cottrell D M. Decomposition of radially and azimuthally polarized beams using a circular-polarization and vortex-sensing diffraction grating. Optics Express, 2010, 18 (7): 7173–7183
47. Zhu J, Chen Y, Zhang Y, Cai X, Yu S. Spin and orbital angular momentum and their conversion in cylindrical vector vortices. Optics Letters, 2014, 39(15): 4435–4438
48. Xiao Q S, Klitis C, Li S M, Chen Y Y, Cai X L, Sorel M, Yu S Y. Generation of photonic orbital angular momentum superposition states using vortex beam emitters with superimposed gratings. Optics Express, 2016, 24(4): 3168–3176
49. Li H, Phillips D B, Wang X, Ho Y L, Chen L, Zhou X, Zhu J, Yu S, Cai X. Orbital angular momentum vertical-cavity surface-emitting lasers. Optica, 2015, 2(6): 547–552

Siyuan Yu received his Bachelor's degree from Tsinghua University, Beijing, China in 1984; Master's degree from Wuhan Research Institute of Post and Telecommunications, Wuhan, China, in 1987; and Ph. D. degree (photonics) from the University of Glasgow, Scotland, UK, in 1997. He is a Professor of Photonic Information Systems at University of Bristol, UK, and a Special Expert Professor at the State Key Laboratory of Optoelectronic Materials and Technologies, Sun Yat-sen University, China.

Prof. Yu has carried out research in the physics and technologies of photonic integration as well as its application in optical networks for over 20 years, focusing on innovative photonic components technologies aimed at addressing key issues at systems and networking levels. He contributed to areas such as high-speed integrated optical switches, micro-cavity lasers, all-optical logic circuits, and integrated quantum photonics. He is currently actively working on integrated photonic devices for the generation and detection of orbital angular momentum modes. He has published more than 150 papers, co-edited a book, and has been granted several international patents.